

ATP Binding Facilitates Target Search of SWR1 Chromatin Remodeler by Promoting One-Dimensional Diffusion on DNA

Claudia C. Carcamo,¹ Matthew F. Poyton,¹ Anand Ranjan,² Giho Park,² Robert K. Louder,² Thuc Dzu,² Carl Wu,² Taekjip Ha^{1,3*}

¹ Department of Biophysics and Biophysical Chemistry, Johns Hopkins University School of Medicine, Baltimore, MD, USA.

² Johns Hopkins University, Department of Biology, 3400 N Charles St, Baltimore, MD 21218, USA.

³ Howard Hughes Medical Institute, Baltimore, MD 21218, USA.

* Corresponding Authors: [*tjha@jhu.edu](mailto:tjha@jhu.edu), [**wuc@jhu.edu](mailto:wuc@jhu.edu)

Abstract

One-dimensional (1D) target search is a well characterized phenomenon for many DNA binding proteins but is poorly understood for chromatin remodelers. Herein, we characterize the 1D scanning properties of SWR1, a yeast chromatin remodeler that performs histone exchange on +1 nucleosomes which are adjacent to a nucleosome depleted region (NDR) at promoters. We demonstrate that SWR1 has a kinetic binding preference for DNA of NDR length as opposed to gene-body linker length DNA. Using single and dual color single particle tracking on DNA stretched with optical tweezers, we directly observe SWR1 diffusion on DNA. We found that various factors impact SWR1 scanning, including ATP which promotes diffusion through nucleotide binding rather than ATP hydrolysis. A DNA binding subunit, Swc2, plays an important role in the overall diffusive behavior of the complex, as the subunit in isolation retains similar, although faster, scanning properties as the whole remodeler. ATP-bound SWR1 slides until it encounters a protein roadblock, of which we tested dCas9 and nucleosomes. The median diffusion coefficient, $0.024 \mu\text{m}^2/\text{sec}$, in the regime of helical sliding, would mediate rapid encounter of NDR-flanking nucleosomes at length scales found in cells.

MAIN TEXT

Introduction

Eukaryotic genomes are packaged into chromatin, the base unit of which is the nucleosome. Both the position of nucleosomes on the genome and their histone composition are actively regulated by chromatin remodeling enzymes (Yen et al., 2012). These chromatin remodelers maintain and modify chromatin architecture which regulates transcription, replication, and DNA repair (Tessarz and Kouzarides, 2014). A particularly well-defined area of chromatin architecture is found at gene promoters in eukaryotes: a nucleosome depleted region (NDR) of about 140 bp in length is flanked by two well-positioned nucleosomes, one of which, the +1 nucleosome, sits on the transcription start site (TSS) (Bernstein et al., 2004; Lee et al., 2007; Xu et al., 2009; Yuan, 2005) and the nucleosome on the opposite side of the NDR, upstream of the TSS, is known as the -1 nucleosome. The +1 nucleosome is enriched for the non-canonical histone variant H2A.Z (Albert et al., 2007; Raisner et al., 2005). In yeast, H2A.Z is deposited into the +1 nucleosome by SWR1 (Swi2/Snf2-related ATPase Complex), a chromatin remodeler in the INO80 family of remodelers (Ranjan et al., 2013). The insertion of H2A.Z into the +1 nucleosome is highly conserved and plays an important role in regulating transcription (Giaimo et al., 2019; Rudnizky et al., 2016).

While the biochemistry of histone exchange has been characterized, the target search mechanism SWR1 uses to preferentially exchange H2A.Z into the +1 nucleosome is not yet understood. The affinity of SWR1 for nucleosomes is enhanced by both long linker DNA (Ranjan et al., 2013; Yen et al., 2013) and histone acetylation (Watanabe et al., 2013; Zhang

et al., 2005), and both factors play a role in the recruitment of SWR1 to promoters. A recent single molecule study further showed that SWR1 likely exploits preferential interactions with long-linker length DNA by demonstrating that H2A.Z is predominantly deposited on the long-linker distal face of the nucleosome (Poyton et al., 2021), similar to what is observed *in vivo* (Rhee et al., 2014). It is possible that SWR1 first binds long-linker DNA and then finds its target, the +1 nucleosome, using facilitated diffusion (**Figure 1A**), as was previously suggested (Ranjan *et al.*, 2013). In a hypothetical facilitated search process SWR1 would first find the NDR through a three-dimensional target search. Once bound, it is possible the entire SWR1 complex diffuses one-dimensionally on the NDR, where it can encounter both the -1 and +1 nucleosomes. Facilitated diffusion has been shown to be essential for expediting the rate at which transcription factors and other DNA binding proteins can bind their target compared to a 3D search alone (Berg et al., 1981; Elf et al., 2007; Hannon et al., 1986; Ricchetti et al., 1988; Von Hippel and Berg, 1989). Furthermore, recently published *in vivo* single particle tracking found that chromatin remodelers have bound-state diffusion coefficients that are larger than that of bound H2A, hinting at the possibility that they may scan chromatin, but those studies could not distinguish between remodeler scanning and locally enhanced chromatin mobility (Kim et al., 2021; Ranjan et al., 2020). It is not known, however, if SWR1 or any other chromatin remodeler can linearly diffuse on DNA, and therefore make use of facilitated diffusion to expedite its target search process. Additionally, SWR1's core ATPase, like other chromatin remodelers, is a superfamily II (SF2) double stranded DNA translocase (Nodelman and Bowman, 2021; Yan and Chen, 2020); while there is no evidence for SWR1 translocation on nucleosomal DNA, it remains possible that SWR1 may undergo directed, instead of diffusional, movements on a DNA duplex in the absence of a nucleosome substrate.

In this study, we used a site-specifically labeled SWR1 complex to demonstrate that SWR1 can scan DNA in search of a target nucleosome. First, we characterized the kinetics of SWR1 binding to DNA and found that the on-rate increases linearly with DNA length while the off-rate is independent of length for DNA longer than 60 bp. Next, we used an optical trap equipped with a scanning confocal microscope to show that SWR1 can diffuse one-dimensionally along stretched DNA, with a diffusion coefficient that permits scanning of a typical NDR in 93 milliseconds. Interestingly, we see that ATP binding alone increases the one-dimensional diffusion coefficient of SWR1 along DNA. We found that a major DNA binding subunit of the SWR1 complex, Swc2, also diffuses on DNA suggesting that it contributes to SWR1's diffusivity on DNA. The diffusion coefficient for both SWR1 and Swc2 increases with ionic strength suggesting that SWR1 utilizes some microscopic dissociation and reassociation events, known as hopping, to diffuse on DNA. However, it is likely that SWR1 only makes infrequent hops, with most of the diffusion on DNA being mediated by helically coupled diffusion, known as sliding, since SWR1 diffusion is blocked by proteins that are bound to DNA, such as dCas9, and the diffusion of the complex is slower than would be expected for majority hopping diffusion. Lastly, we observed SWR1 diffusion on DNA containing sparsely deposited nucleosomes and found that SWR1 diffusion is confined between nucleosomes. Our data indicates that a multi-subunit chromatin remodeler can diffuse along DNA and suggests that SWR1 finds its target, the +1 nucleosome, through facilitated diffusion. Facilitated diffusion may be a common search mechanism for all chromatin remodelers that act upon nucleosomes positioned next to free DNA, such as those adjacent to the NDR.

Results

SWR1 binding kinetics depend on DNA length

101 To study both the DNA binding kinetics and diffusive behavior of SWR1, we
102 generated a site-specifically labeled complex referred to as Cy3-SWR1 (**Figure 1B**). We
103 purified SWR1 from *S. cerevisiae* in the absence of the Swc7 subunit (SWR1 Δ Swc7).
104 Recombinant Swc7 was expressed and purified from *E. coli*, a single cysteine in Swc7 was
105 labeled with Cy3, and the labeled Swc7 was then added to the SWR1 Δ Swc7 preparation
106 between two steps of the traditional tandem affinity purification protocol (Sun et al., 2020).
107 Subsequent purification on a glycerol gradient revealed that the Cy3-labeled Swc7
108 co-migrated with the rest of the SWR1 subunits, demonstrating incorporation of Swc7 back
109 into the SWR1 complex (**Figure S1A**). The histone exchange activity of the labeled
110 Cy3-SWR1 was identical to that of wild type SWR1 as revealed by an electrophoretic
111 mobility shift assay (EMSA) (**Figure S1B**).

112 While it is well established that the affinity of SWR1 for DNA is dependent on DNA
113 length (Ranjan *et al.*, 2013), the kinetics of binding are unknown. We used single-molecule
114 colocalization measurements to observe Cy3-SWR1 binding and unbinding on Cy5-labeled
115 DNA of different lengths in real time (**Figure 1C-E**). These measurements showed that both
116 the on-rate (k_{bind}) and the lifetime of the SWR1-DNA complex (t_{off}) are dependent on DNA
117 length. The on-rate for SWR1 binding to 20 bp DNA, the approximate size of linker DNA
118 between intragenic nucleosomes in yeast, was $1 \times 10^6 \text{ M}^{-1} \text{ s}^{-1}$. Increasing the DNA length to
119 150 bp, the approximate size of the NDR in yeast, increases the binding rate 36-fold to
120 $3.6 \times 10^7 \text{ M}^{-1} \text{ s}^{-1}$. k_{bind} increased linearly with DNA length between these two values
121 (**Figure 1F**). Interestingly, we found that DNA could accommodate multiple bound SWR1
122 molecules, with the likelihood of multiple binding events increasing with DNA length (see
123 **Figure 1E** for example trace). Cy3-Swc7 alone exhibited no affinity for 150 bp DNA (data
124 not shown), suggesting that the observed Cy3-signal increase is caused by the full Cy3-
125 SWR1 complex binding to DNA.

126 The lifetime of SWR1 bound to DNA (t_{off}) was also sensitive to DNA length,
127 exhibiting two sharp increases as DNA size increased from 20 to 40 bp, and 60 to 80 bp.
128 Whereas t_{off} for 20 bp DNA was $1.5 \pm 0.3 \text{ s}$, t_{off} for SWR1 binding to 40 and 60 bp DNA
129 increased to $9 \pm 1.4 \text{ s}$ and $12 \pm 5.8 \text{ s}$, respectively, which is the same within error
130 (**Figure 1G**). Once the DNA was 80 bp or longer, however, the lifetime increased
131 dramatically to at least 30 s, which is the photobleaching limit of the measurement
132 (**Figure S1C**). Measurements at low laser power showed that SWR1 remained bound to
133 150 bp DNA for at least 5 minutes. t_{off} was unchanged in the presence of ATP but was
134 sensitive to ionic strength, decreasing with added salt (**Figure 1D-E**). Curiously, t_{off} also
135 decreased in the presence of competitor DNA (**Figure S1D-E**). The kinetic measurements
136 show that the affinity of SWR1 for DNA greater than 60 bp is primarily limited by the
137 on-rate, suggesting the increased occupancy of SWR1 at longer NDRs observed in yeast

138
139

(Ranjan *et al.*, 2013) is a result of the increased probability of SWR1 finding the NDR, as opposed to an increase in the residence time of SWR1.

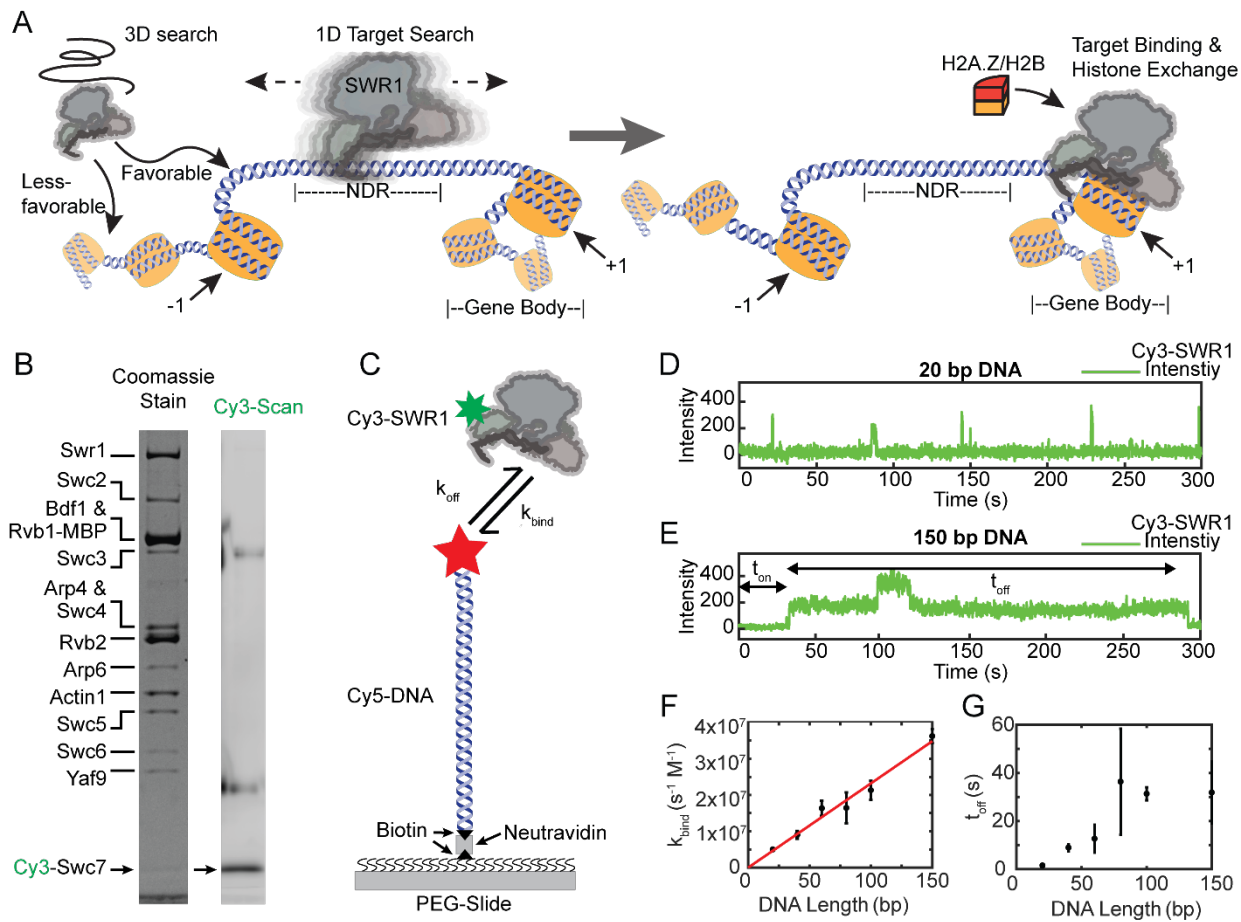


Fig. 1. SWR1 binds DNA in short and long-lived states and prefers longer DNAs. (A) Proposed facilitated search mechanism for how SWR1 locates the +1 nucleosome. (B) A denaturing SDS-PAGE of reconstituted Cy3-SWR1 imaged for Coomassie (left) and Cy3 fluorescence (right). Cy3-Swc7 is faint when stained with Coomassie but is a prominent band in the Cy3 scan. The two diffuse bands that run at higher molecular weight and appear in the Cy3 scan are carry over from the ladder loaded in the adjacent lane. (C) A schematic for the single-molecule colocalization experiment where the kinetics of Cy3-SWR1 binding to Cy5-labeled DNA of different lengths was measured. (D-E) Representative trace for Cy3-SWR1 binding to (D) 20 bp Cy5-DNA, and to (E) 150 bp DNA. A second Cy3-SWR1 can be seen binding at approximately 100 s. (F) Measured binding time (k_{bind}) for SWR1 to DNA of different lengths. The red line is a linear fit to the data. (G) The lifetime (t_{off}) of Cy3-SWR1 bound to DNAs of different lengths.

140 *SWR1 scans DNA*

141 To determine if SWR1 can move along DNA, we tracked single Cy3-SWR1
142 complexes bound to stretched lambda DNA using an optical trap equipped with a confocal
143 scanning microscope (LUMICKS, C-Trap) (Heller *et al.*, 2014a; Heller *et al.*, 2014b). The
144 experiment was carried out using a commercial flow-cell in order to efficiently catch beads,
145 trap DNA, and image bound proteins over time (Figure 2A) as has been performed
146 previously (Brouwer *et al.*, 2016; Gutierrez-Escribano *et al.*, 2019; Newton *et al.*, 2019; Rill
147 *et al.*, 2020; Wasserman *et al.*, 2019). Briefly, lambda DNA end-labeled with biotin is
148 tethered between two optically trapped streptavidin-coated polystyrene beads, pulled to
149 5 piconewton (pN) tension to straighten the DNA (Baumann *et al.*, 2000) and the distance
150 between the two optical traps is clamped (Figure 2A-B). After confirming the presence of
151 a single DNA tether, the DNA is brought into an adjacent channel of the flow-cell containing

152 250 picomolar Cy3-SWR1. Confocal point scanning across the length of the DNA was used
 153 to image single Cy3-SWR1 bound to lambda DNA over time to generate kymographs
 154 (**Figure 2B-C**). The observed fluorescent spots represent the Cy3-SWR1 complex as
 155 Cy3-Swc7 alone was unable to bind DNA (**Figure S2**).

156 Cy3-SWR1 bound to lambda DNA is mobile, demonstrating that Cy3-SWR1 can
 157 move on DNA once bound and the movement did not appear to be unidirectional. Therefore,
 158 we plotted mean square displacement (MSD) vs time and found that the initial portion of
 159 the curve is linear, suggesting diffusional movements (**Figure 2D**). The diffusion
 160 coefficient observed ($D_{1,obs}$) for Cy3-SWR1 was $0.013 \pm 0.002 \mu\text{m}^2/\text{sec}$ in buffer alone
 161 (**Figure 2E-F**). Since the distributions are non-normal, $D_{1,obs}$ is defined as the median
 162 diffusion coefficient of all molecules in a condition; individual diffusion coefficients were
 163 determined from the slope of the initially linear portion of their respective MSD plot (see
 164 **Materials and Methods** for more details). This diffusion coefficient is comparable to other

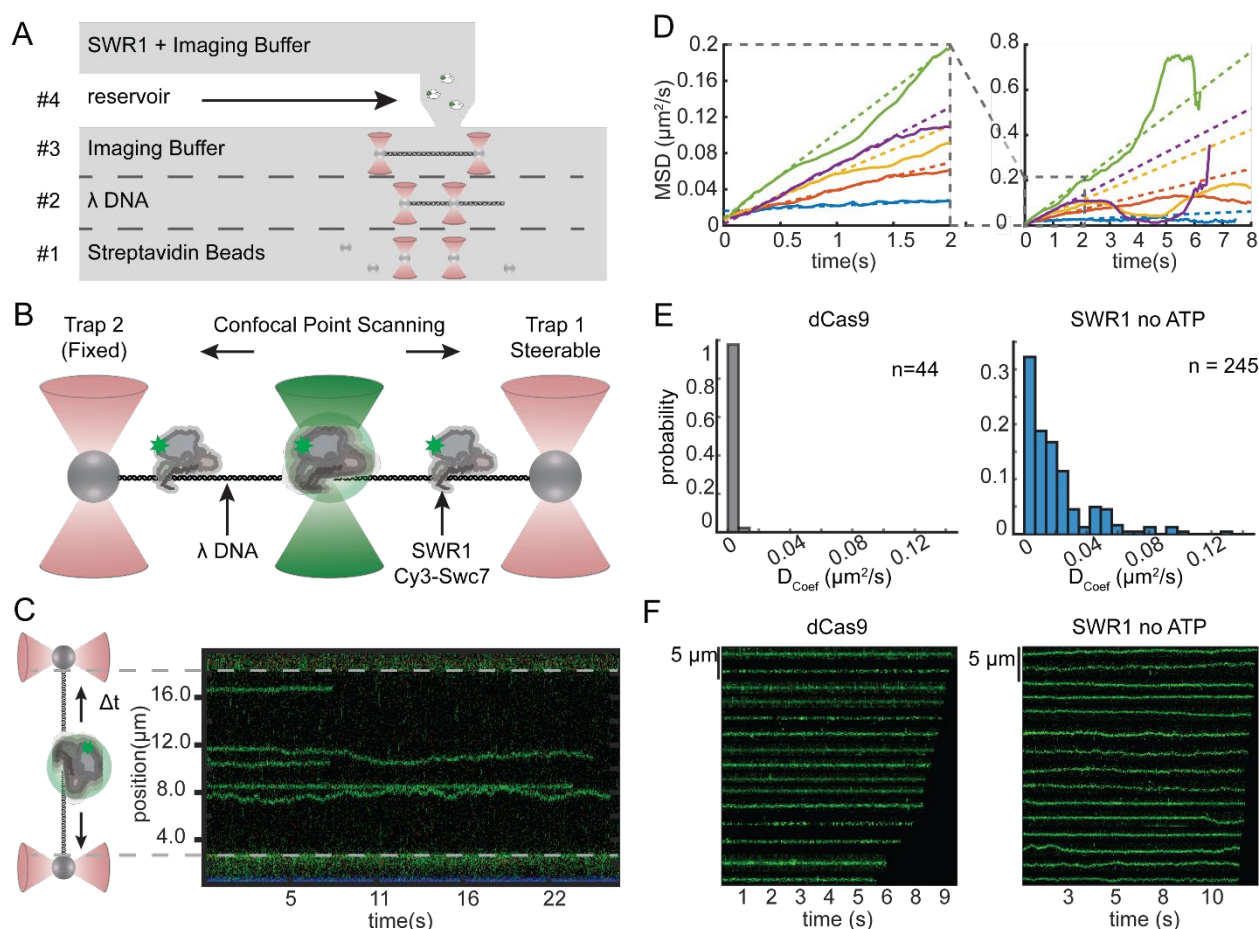


Fig. 2. SWR1 diffuses on extended dsDNA. (A) Schematic representation of a C-Trap microfluidics imaging chamber with experimental workflow depicted therein: #1 catch beads, #2 catch DNA, #3 verify single tether, #4 image SWR1 bound to DNA. (B) Schematic representation of confocal point scanning across the length of lambda DNA tethered between two optically trapped beads. This method is used to monitor the position of fluorescently labeled SWR1 bound to DNA. (C) Example kymograph with a side-by-side schematic aiding in the interpretation of the kymograph orientation. (D) Mean squared displacement (MSD) versus time for a random subset of SWR1 traces in which no ATP is added. An enlargement of the initial linear portion is shown to the left where colored dashed lines are linear fits to this portion. (E) Histogram of diffusion coefficients for dCas9 (left) and SWR1 in which no ATP is added (right) (F) Segmented traces of dCas9 (left) and SWR1 in which no ATP is added (right).

165 proteins with characterized 1D diffusion (Gorman et al., 2007; Park et al., 2021). In contrast
 166 $D_{1,obs}$ for specifically bound Cy5-dCas9, which is immobile, is $0.0003 \pm 0.0004 \mu\text{m}^2/\text{sec}$,
 167 which is forty times lower than Cy3-SWR1. These measurements clearly show that SWR1
 168 undergoes Brownian diffusion on nucleosome-free DNA.

169 *ATP bound SWR1 is more diffusive than the unbound complex*

170 To determine if SWR1 can actively translocate on DNA, we observed the motion of
 171 Cy3-SWR1 in the presence of 1 mM ATP (**Figure 3**). The MSDs of Cy3-SWR1 in the
 172 presence of ATP remained linear, showing that SWR1 does not translocate directionally on
 173 DNA (**Figure 3A**). The increased slope of the MSDs in the ATP condition, however, does
 174 indicate that ATP increases the diffusion. This is further observed in an overlay of 10
 175 random trajectories of SWR1 with and without ATP, which demonstrates that SWR1
 176 diffuses a greater distance from the starting position in the presence of ATP and that its
 177 motion is not directional (**Figure 3B**). To address whether this increased diffusion was due
 178 to ATP hydrolysis, we also measured SWR1 diffusion in the presence of 1 mM ATP γ S, a
 179 nonhydrolyzable analog of ATP, as well as with ADP. The distribution in diffusion
 180 coefficients in the presence of ATP and ATP γ S are both shifted to higher values compared
 181 to in the absence of ATP or in the presence of ADP (**Figure 3C**). This shift was shown to
 182 be statistically significant using the non-parametric Mann-Whitney U-test (**Figure 3D**).
 183 SWR1 diffusion in the presence of 1mM ATP ($D_{1,obs} = 0.024 \mu\text{m}^2/\text{sec} \pm 0.001$) was not
 184 significantly different than diffusion in the presence of 1 mM ATP γ S
 185 ($D_{1,obs} = 0.026 \mu\text{m}^2/\text{sec} \pm 0.002$). Similarly, SWR1 diffusion in the absence of ATP

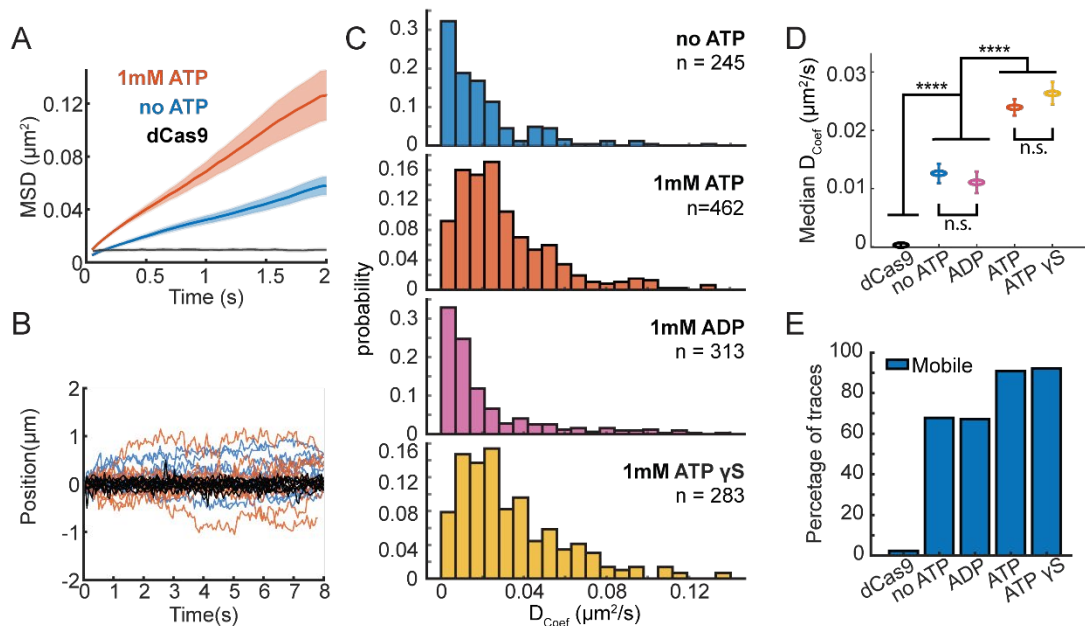


Fig. 3. ATP binding modulates SWR1 diffusion. (A) Mean MSD vs time plotted for 1mM ATP (orange), no ATP (blue), and dCas9 (black) with shaded error bars SEM. (B) SWR1 trajectories aligned at their starts for 1mM ATP (orange lines), no ATP (blue lines), and dCas9 as reference for immobility (black lines). 10 random traces shown per sample. (C) Histograms of diffusion coefficients extracted from individual trajectories for SWR1 diffusion in the presence of no ATP, 1mM ATP, 1mM ADP, 1mM ATP γ S (from top to bottom). The number of molecules measured (n) for each condition is printed in each panel. (D) Median diffusion coefficients for SWR1 in varying nucleotide conditions. dCas9 is shown as a reference. Error bars are the uncertainty of the median. (E) Percentage of mobile traces in each condition, where immobility is defined as traces with similar diffusion coefficients to dCas9 (defined as diffusion coefficients smaller than $0.014 \mu\text{m}^2/\text{sec}$).

($D_{1,obs} = 0.013 \mu\text{m}^2/\text{sec} \pm 0.002$) was not different than SWR1 diffusion in the presence of 1mM ADP ($D_{1,obs} = 0.011 \mu\text{m}^2/\text{sec} \pm 0.002$). Additionally, we found that ATP decreased the fraction of slow or immobile Cy3-SWR1 molecules, defined as those molecules that show D_1 values that are indistinguishable from dCas9 values (**Figure 3E**). While 9% of Cy3-SWR1 were slow or immobile in the presence of ATP, 32% were slow or immobile in buffer alone. These results show that while SWR1 does not actively translocate on DNA, ATP binding alone increases the mobility of SWR1 on DNA.

SWR1 and the DNA binding domain of the Swc2 subunit slide on DNA

SWR1 binding to DNA is mediated in part by the Swc2 subunit, which harbors a positively charged and unstructured DNA binding domain (Ranjan *et al.*, 2013). To determine if Swc2 contributes to the diffusive behavior of SWR1 on DNA we compared diffusion of the SWR1 complex to diffusion of the DNA binding domain (DBD) of Swc2 (residues 136-345, **Figure S3**). We found that Swc2 also diffuses on DNA, however the median diffusion coefficient, $D_{1,obs} = 1.04 \mu\text{m}^2/\text{sec} \pm 0.09$, was approximately 40-fold larger than that of SWR1 in the presence of 1mM ATP (**Figure 4, Materials and Methods**). This large difference in measured diffusion coefficients could be due to the difference in size between the small Swc2 DBD and full SWR1 complex or to other DNA binding components of SWR1 interacting with DNA and increasing friction. Based on theoretical models of rotation coupled versus uncoupled diffusion, the scaling relationship between size and

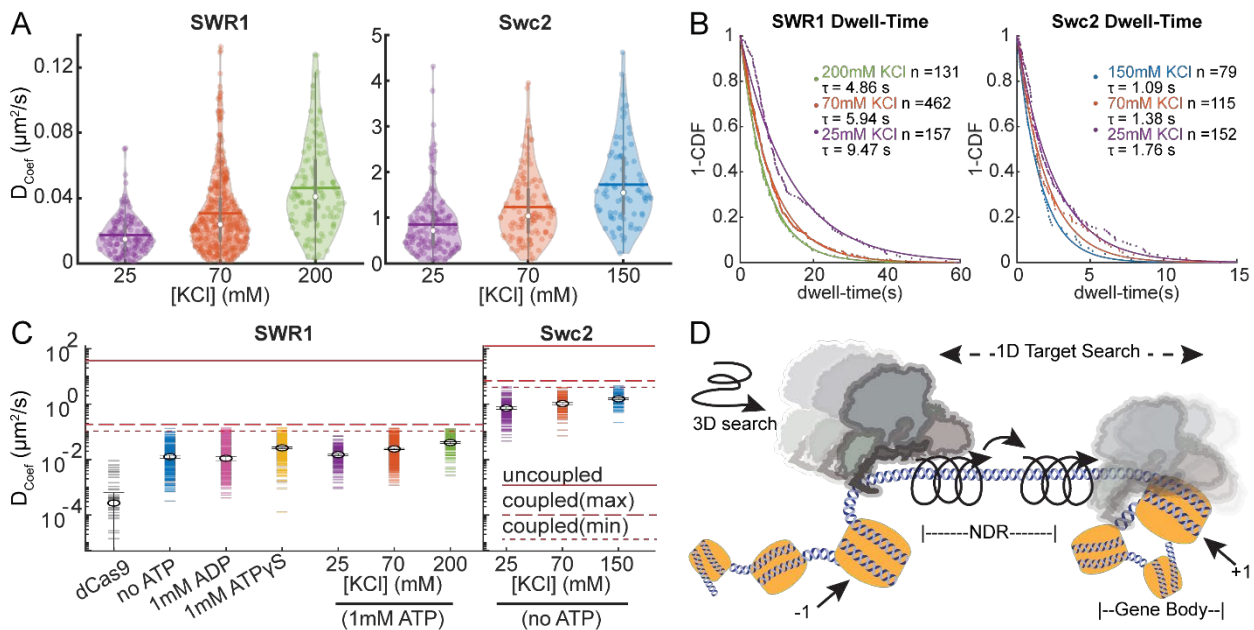


Fig. 4. SWR1 and Swc2 DBD utilize sliding to scan DNA. (A) Violin plots of diffusion coefficients for SWR1 and Swc2 DNA binding domain (DBD) in increasing potassium chloride concentrations. Medians are shown as white circles and the mean is indicated with a thick horizontal line. (B) 1-CDF plots of SWR1 and Swc2 were fit to exponential decay functions to determine half-lives of binding in varying concentrations of potassium chloride. The number of molecules as well as half-lives determined are printed therein. Dots represent data points, while solid lines represent fits. Half-lives are calculated using the length of all the trajectories in each condition. (C) Upper limits for diffusion of SWR1 and Swc2 predicted using either a helically uncoupled model for hopping diffusion (uppermost solid red line) or a helically coupled model for sliding diffusion (lower dashed red lines). Two dashed lines are shown for helically coupled upper limits because the distance between the helical axis of DNA and the center of mass of either SWR1 or Swc2 is unknown. Markers represent median values. (D) A schematic representation of a model for how SWR1 likely performs 1D diffusion on DNA.

206 diffusion coefficient is consistent with SWR1 and Swc2 DBD utilizing rotationally-coupled
207 sliding (Blainey *et al.*, 2009) (**Figure S4**).

208 Next, we found that both SWR1 and Swc2 DBD show increased diffusion with
209 increasing concentrations of potassium chloride (**Figure 4A**), and each showed decreasing
210 binding lifetimes with increasing salt (**Figure 4B**). Both increased diffusion and decreased
211 binding lifetimes are features of 1D hopping, as the more time a protein spends in
212 microscopic dissociation and reassociation the faster it can move on DNA, but also falls off
213 DNA more frequently (Bonnet *et al.*, 2008; Mirny *et al.*, 2009). This data is consistent with
214 the single molecule TIRF data presented earlier (**Figure S1E**), which also reveals decreased
215 binding lifetimes to DNAs when ionic strength is increased. The TIRF assay also shows that
216 competitor DNA can decrease binding lifetime as would be expected for a protein that hops
217 on DNA and may be prone to alternative binding onto competitor DNA (Brown *et al.*, 2016;
218 Gorman *et al.*, 2007).

219 The theoretical upper limit of diffusion for a particle that uses linear translocation
220 (1D hopping) is higher than the theoretical upper limit of diffusion with helically coupled
221 sliding because in the latter there are additional rotational components of friction incurred
222 when circumnavigating the DNA axis (Blainey *et al.*, 2009). Based on the molecular weight
223 of SWR1 and Swc2, the theoretical upper limits of 1D diffusion using rotation coupled
224 versus uncoupled 1D diffusion can be calculated (**Materials and Methods**). In all
225 conditions measured, the median diffusion of SWR1 is below the upper limit with rotation
226 (**Figure 4C**), consistent with much of the observed diffusion coming from SWR1 engaging
227 in rotationally coupled diffusion. Nonetheless, some individual traces have diffusion
228 coefficients that surpass this theoretical maximum, indicating that there may be alternative
229 modes for engaging with DNA (e.g., infrequent hopping), which allows it to surpass this
230 limit (Gorman *et al.*, 2010). A similar phenomenon was observed for Swc2 DBD, which
231 also exhibited median diffusion coefficients below the theoretical maximum with rotation,
232 with some traces having diffusion coefficients above this limit (**Figure 4C**). These trends
233 are consistent with a model in which SWR1 utilizes occasional hopping, while using
234 1D helically coupled sliding as the major mode of diffusion (**Figure 4D**).

235 *SWR1 cannot bypass bound dCas9*

236 While the nucleosome depleted region is a region of open chromatin where
237 accessibility to DNA is higher compared to DNA in gene bodies, SWR1 must compete with
238 transcription factors and other DNA binding proteins for search on this DNA (Kim *et al.*,
239 2021; Kubik *et al.*, 2019; Nguyen *et al.*, 2021; Rhee and Pugh, 2012). Proteins that diffuse
240 on DNA by 1D hopping have been shown to be capable of bypassing protein barriers and
241 nucleosomes (Gorman *et al.*, 2010; Hedglin and O'Brien, 2010). To investigate whether
242 ATP bound SWR1 can bypass protein barriers, we turned to dCas9, an endonuclease
243 inactive mutant of Cas9, to serve as a programmable barrier to diffusion. We used a dual
244 color single particle tracking scheme to simultaneously observe Cy3-labeled SWR1
245 diffusion and the positions of Cy5-labeled dCas9 (**Figure 5**). crRNAs were used to direct
246 dCas9 binding to 5 positions on the lambda DNA using previously validated targeting
247 sequences (**Figure 5A, Table S1, Materials and Methods**) (Sternberg *et al.*, 2014). We
248 assume that dCas9 binding far outlasts the photobleaching lifetime of Cy5 (Singh *et al.*,
249 2016), therefore we use the average position of the particle to extend the trace after
250 photobleaching of Cy5 for colocalization analysis. Out of 107 traces with colocalization
251 events, 67% showed SWR1 moving away from dCas9 toward where it came from as if it
252 was reflected from a boundary (**Figure 5B, D**). Another 30% of traces showed SWR1

253
254
255
256
257
258

immobile and colocalized with dCas9 for the duration of the trace (**Figure 5C, D**). Only 3% of all colocalization events exhibited a cross-over event (**Figure 5D, S5**). The ability of dCas9 to block SWR1 diffusion in most encounters further supports a model in which SWR1 mainly engages in helically coupled sliding (**Figure 4D**). Infrequent hopping events that colocalize to a dCas9 encounter may contribute to the presence of the rare bypass event (**Figure S5**).

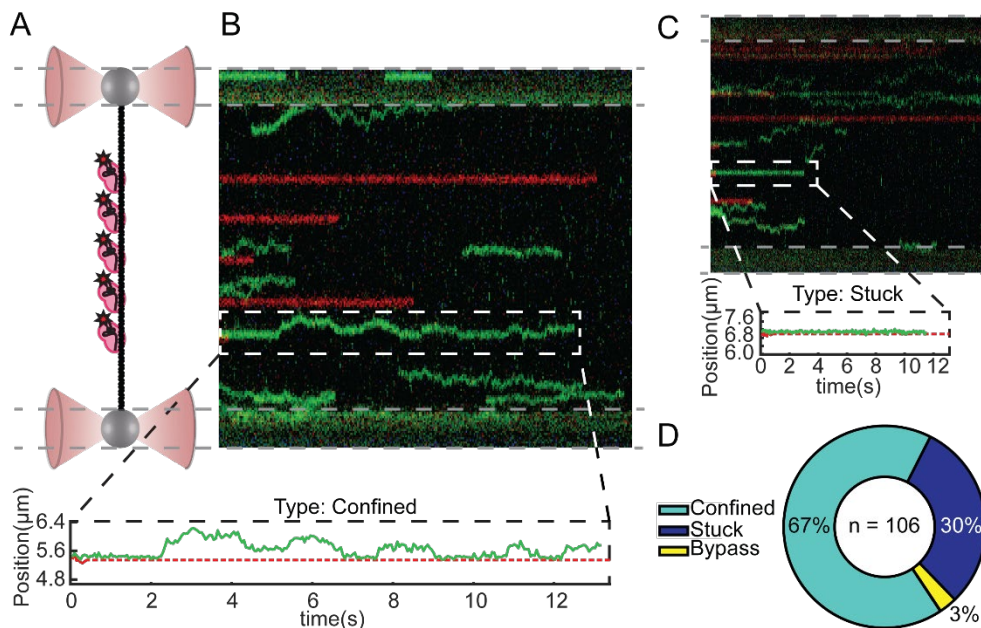


Fig. 5. SWR1 protein roadblock bypass assay. (A) A schematic of the experimental set-up: 5 Cy5-labeled gRNA position dCas9 at 5 evenly spaced sites along lambda DNA. When SWR1 encounters dCas9 during 1D scanning, there are three main types of colocalization events observed. (B-C) Example kymographs including trajectories for two common types of colocalization observed during SWR1 encounter with dCas9. (B) SWR1 diffusion is confined by dCas9. (C) SWR1 becomes stuck to the dCas9 and is no longer diffusive. In the example trajectories, dCas9 is represented as a dashed red line after Cy5 has photobleached, however due to long binding lifetime of dCas9 we continue to use its position for colocalization analysis. (D) Pie-chart of the three types of colocalization events with the total number of observations printed therein.

259
260
261
262
263
264
265
266
267
268
269
270
271
272
273
274
275

Nucleosomes are barriers to SWR1 diffusion

Diffusion over nucleosomes may also be an important aspect of target search; it is not known whether SWR1 diffusing on an NDR would be confined to this stretch of DNA by flanking +1 and -1 nucleosome(s) or whether its diffusion could continue into the gene body. To investigate this, we monitored SWR1 diffusion on sparse nucleosome arrays reconstituted on lambda DNA. Nucleosomes were formed at random sites along lambda DNA using salt gradient dialysis, as has been done previously (Gruszka et al., 2020; Visnapuu and Greene, 2009) (**Figure S6, Materials and Methods**). On average, 36 ± 15 nucleosomes were incorporated onto the lambda nucleosome arrays as shown by nucleosome unwrapping force-distance curves (**Figure 6A-B**); nucleosomes showed detectable unwrapping at forces greater than 15 pN (Brower-Toland et al., 2002; Fierz and Poirier, 2019), and these unwrapping events were used to confirm the number of nucleosomes on the array which is determined using the length of the array at 5pN (see **Materials and Methods**). Overall, the behavior of SWR1 on lambda nucleosome arrays was notably different than on naked lambda DNA (**Figure 6C-D**). The mean MSD for SWR1 on naked DNA increases linearly with time at short time scales (< 2 s), whereas the mean MSD for SWR1 on the lambda nucleosome array plateaus over this same time scale,

276 indicative of confined 1D diffusion (**Figure 6D**). The degree to which diffusion is confined
277 can be described by $\alpha < 1$ where $MSD = Dt^\alpha$. Whereas SWR1 on naked DNA has an $\alpha = 0.88$
278 over a 2 second time scale, SWR1 on the lambda array has an $\alpha = 0.089$ reflecting
279 considerable confinement. By fitting the MSD curve to an exponential function, the mean
280 MSD appears to approach a limit of $0.054 \mu\text{m}^2$ (**Figure S7**). Assuming an even distribution
281 of an average of 36 nucleosomes per array (**Figure 6B**), the mean distance between
282 nucleosomes is equal to $0.38 \mu\text{m}$; whereas the length of DNA to which SWR1 diffusion is
283 confined is approximately $0.23 \mu\text{m}$, determined from the square root of the MSD limit
284 described above. The data, therefore, suggests that SWR1 diffusion is confined to the space
285 between nucleosomes.

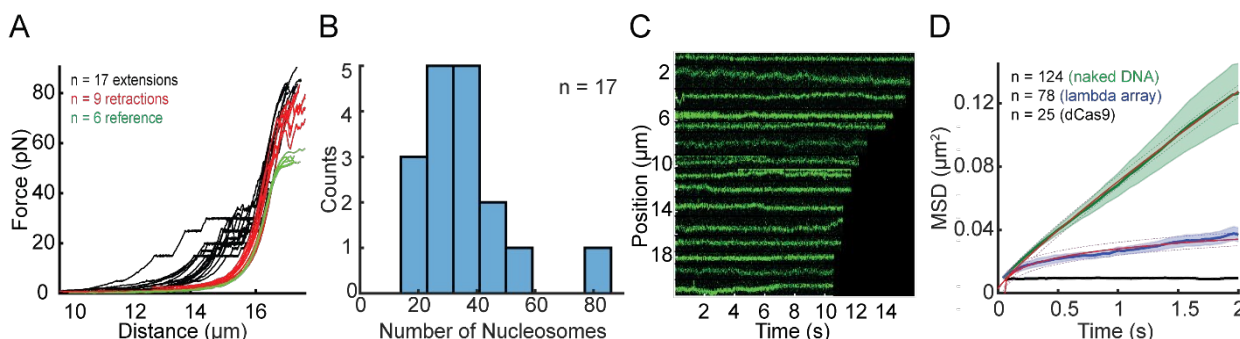


Fig. 6. SWR1 does not diffuse over nucleosomes. (A) Lambda nucleosome arrays are pulled to $> 15\text{pN}$ tension, at which point nucleosomes begin to unwrap. Black curves are unwrapping curves where the force is clamped at either 20, 25 or 30 pN to visualize individual unwrapping events; red curves are the collapse of the DNA after unwrapping nucleosomes; green curves are reference force extension plots of lambda DNA without nucleosomes. (B) Histogram of the number of nucleosomes per array. (C) Representative SWR1 particles diffusing on the nucleosome arrays are cropped and arranged by the length of the trace. (D) Mean MSDs are fit over the first 2 seconds to $MSD = Dt^\alpha$, where α is used to quantify the degree of confinement of the trace, and the red lines represent the fits. MSD as a function of time with shaded error bars representing SEM for SWR1 diffusing on naked DNA [green curve, $\alpha = 0.88$] as compared to SWR1 diffusing on lambda nucleosome arrays [blue, $\alpha = 0.089$] and dCas9 [black].

286 Discussion

287 Reducing the dimensionality of nucleosome target search

288 Our single molecule tracking data shows that SWR1 slides on DNA, which is a novel
289 finding for a chromatin remodeler. Moreover, SWR1 scans DNA with a diffusion
290 coefficient comparable to other well-characterized proteins that utilize facilitated diffusion
291 to bind specific DNA sequences or lesions (Ahmadi et al., 2018; Blainey et al., 2006;
292 Gorman et al., 2010; Kamagata et al., 2020; Porecha and Stivers, 2008; Tafvizi et al., 2011;
293 Tafvizi et al., 2008; Vestergaard et al., 2018). Without 1D sliding, the search process of
294 SWR1 for its target nucleosome would be dependent solely on 3D collisions with
295 nucleosomes. In the yeast genome, there are approximately 61,568 annotated nucleosomes
296 (Jiang and Pugh, 2009; Kubik et al., 2015), of which 4,576 are identified as potential
297 +1 nucleosomes enriched in H2A.Z (Tramantano et al., 2016). Since only 7% of
298 nucleosomes are targets of SWR1 histone exchange, we believe that +1 nucleosomes use
299 their adjacent NDRs as antennas, promoting SWR1 binding and 1D search to encounter
300 flanking nucleosomes (Mirny et al., 2009). This increased efficiency in target localization
301 through dimensional reduction of the search process may be one that could extend to other
302 chromatin remodelers that act on nucleosomes adjacent to the NDR, such as RSC,
303 SWI/SNF, CHD1, ISW1, ISW2, and INO80 (Kim et al., 2021).

304 *ATP binding facilitates SWR1 target search and diffusion on DNA*

305 We observed that SWR1 diffusion is increased in the presence of ATP, and that
306 substitution with ATP γ S also results in similar increased diffusion suggesting that this
307 enhancement is mediated by nucleotide binding rather than hydrolysis. SWR1 requires ATP
308 to perform the histone exchange reaction, and basal levels of ATP hydrolysis when any one
309 of the required substrates for the histone exchange reaction is missing is low (Luk et al.,
310 2010). This includes the scenario where SWR1 is bound to DNA in the absence of the
311 nucleosome and H2A.Z/H2B dimer. Therefore, we do not expect SWR1 diffusion in the
312 presence of 1mM ATP to be modulated by ATP hydrolysis, which is consistent with our
313 findings. Binding of nucleotide cofactor has been shown to produce conformational changes
314 in ATPases that can affect their diffusion on DNA (Gorman *et al.*, 2007). The core ATPase
315 domain of SWR1, Swr1, like other chromatin remodelers, belongs to the superfamily 2
316 (SF2) of translocases which are known to have two lobes that switch between an open and
317 closed conformation with ATP binding and hydrolysis (Beyer et al., 2013; Nodelman et al.,
318 2020). It is therefore possible that the ATP bound closed conformation of the core ATPase
319 results in a DNA binding interface, distributed across accessory domains, that is more
320 conducive to diffusion on DNA, contributing to the enhanced diffusion of SWR1 in the
321 presence of ATP or ATP γ S. In the present study we further investigated SWR1's main
322 DNA binding subunit, Swc2, which forms an extended interface with the core
323 ATPase (Willhoft et al., 2018). In addition to the changes in the contacts that the translocase
324 domain makes with DNA in the closed versus open form, it is possible that ATP modulates
325 how Swc2 engages with the DNA through conformational changes propagated from Swr1.
326 Swc2 appears to be an important accessory subunit for 1D diffusion, as we were able to
327 show that in isolation, the DNA binding domain of Swc2 slides on DNA with properties
328 similar to that of the whole complex although with a much-increased diffusion coefficient.

329 Conformations that result in slower sliding presumably become trapped in free
330 energy minima along the DNA where the DNA sequence or the presence of DNA lesions
331 results in a more stably bound DNA-protein interaction (Gorman *et al.*, 2007). While it
332 remains unknown whether SWR1 interacts with different sequences of DNA differently in
333 the context of sliding, we believe this may be a possibility since we observe a distribution
334 in diffusion coefficients within any single condition which would not be expected if the
335 energetic costs of binding substrate were equal everywhere. The NDR is rich in AT-content;
336 therefore one might imagine that SWR1 may have evolved to be better at scanning DNA
337 with high AT-content (Chereji et al., 2018). Lambda DNA, the DNA substrate used in this
338 study, has asymmetric AT-content, which has been shown to affect nucleosome positioning
339 during random deposition (Visnapuu and Greene, 2009). Future studies of chromatin
340 remodeler 1D diffusion are needed to address this possibility.

341 *SWR1 and Swc2 predominantly slide with diffusion confined between roadblocks*

342 The way in which a protein engages with DNA during 1D search can have impacts
343 on both scanning speed and target localization. For instance, a protein that maintains
344 continuous contact with the DNA in part through charge-charge interactions with the
345 phosphate backbone will predominantly utilize helically coupled sliding. By contrast, a
346 protein that dissociates just far enough from the DNA for cation condensation on the
347 phosphate backbone to occur before quickly reassociating will utilize linear hopping to
348 perform short 3D searches before reassociating at a nearby site on the DNA (Mirny *et al.*,
349 2009). Proteins that hop on DNA therefore have increased diffusion with increased
350 monovalent cation concentration, as a higher screening potential results in more frequent
351 hops. SWR1 and the DNA binding domain of the Swc2 subunit both become more diffusive
352 as the concentration of potassium chloride is increased (**Figure 4A**), which indicates that
353 both utilize some degree of hopping when diffusing on DNA.

354 Nonetheless, the observed diffusion for both SWR1 and Swc2, on average, falls
355 within a range expected for a protein that predominantly uses a sliding mechanism to diffuse
356 on DNA. In order for a protein to slide or hop on DNA, the energy barrier (ΔG^\ddagger) to break
357 the static interaction and dynamically engage with the DNA following the parameters of
358 either the sliding or hopping model must be less than $\approx 2 k_B T$ (Ahmadi *et al.*, 2018; Gorman
359 *et al.*, 2007; Slutsky and Mirny, 2004). Based on the molecular weight of SWR1 and Swc2,
360 the upper limit of 1D diffusion was estimated for both the sliding and hopping model
361 (**Figure 4C, Materials and Methods**). The upper limit of diffusion coefficients for
362 rotation-coupled sliding-only diffusion is lower than hopping-only diffusion due to the
363 rotational component increasing friction in the sliding model. We found that most particles
364 for either SWR1 or Swc2 fall below the estimated upper limit for sliding diffusion. This
365 observation indicates that, averaged over the length of the trace, the energetic barrier to
366 exclusively hop along DNA is too large, whereas the energy barrier for sliding diffusion is
367 permissive ($< 2 k_B T$). Therefore, while both SWR1 and Swc2 DNA binding domain can
368 engage in hopping, both on average utilize sliding diffusion as exhibited by their slow
369 diffusion.

370 Sliding as a predominant component of the SWR1 interaction with DNA is further
371 evidenced by the observation that SWR1 can neither bypass a dCas9 protein roadblock nor
372 nucleosomes with high efficiency. Other studies have found that proteins that utilize sliding
373 as the predominant form of 1D diffusion cannot bypass proteins or nucleosomes (Brown *et al.*,
374 2016; Gorman *et al.*, 2010; Hedglin and O'Brien, 2010), whereas a protein that
375 predominantly hops may be able to bypass these obstacles. The utilization of hopping
376 diffusion has been described as a trade-off between scanning speed and accuracy, with
377 proven implications in target sequence bypass by the transcription factor LacI (Marklund *et al.*,
378 2020). Whether the same may be true for chromatin remodelers in search of specific
379 nucleosomes is yet to be reported.

380 381 *Concluding remarks*

382 Single particle tracking in vivo has shown that approximately 47% of SWR1
383 molecules are bound to chromatin and the remainder is performing 3D diffusion (Ranjan *et al.*,
384 2020). Once bound (e.g. near the center of an average NDR of ~ 150 bp) our findings
385 suggest that SWR1 would require 46 milliseconds (see **Materials and Methods**) to scan
386 and encounter a flanking nucleosome by 1D diffusion at $0.024 \mu m^2/sec$. A recent report
387 shows that when complexed with a canonical nucleosome and the H2A.Z-H2B dimer,
388 SWR1 can rapidly perform the ATP hydrolysis-dependent histone exchange reaction, which
389 occurs on average in 2.4 seconds as measured by an in vitro single molecule FRET assay
390 (Poyton *et al.*, 2021). Thus, SWR1-catalyzed histone H2A.Z exchange on chromatin may
391 be an intrinsically rapid event that occurs on a timescale of seconds. While 1D diffusion
392 should in principle allow SWR1 to encounter either the +1 or -1 nucleosome at the ends of
393 the NDR, directionality may be conferred by the preferentially acetylated +1 nucleosome,
394 where interaction with SWR1's bromodomain should increase binding lifetime during
395 encounter events (Ranjan *et al.*, 2013). Future studies of 1D diffusion with the use of
396 nucleosome arrays that mimic the natural nucleosome arrangement and histone
397 modifications of NDRs and gene bodies should provide important physical and temporal
398 insights on how SWR1 undergoes target search to capture its nucleosome substrates at gene
399 promoters and enhancers. Extension of this approach to other ATP-dependent chromatin
400 remodelers and histone modification enzymes will facilitate understanding of the
401 cooperating and competing processes on chromatin resulting in permissive or
402 nonpermissive architectures for eukaryotic transcription.

404 **Materials and Methods**

405 *Protein purification, fluorescence labeling, and functional validation (SWR1 & Swc2)*

406 The SWR1 complex labeled only on Swc7 was constructed as has been previously
407 documented (Poyton *et al.*, 2021). We demonstrated that the fluorescently labeled SWR1
408 complex maintains full histone exchange activity (**Figure S1B**). For this assay, 1 nM SWR1,
409 5 nM nucleosome, and 15 nM ZB-3X flag were combined in standard SWR1 reaction buffer
410 [25 mM HEPES pH 7.6, 0.37 mM EDTA, 5% glycerol, 0.017% NP40, 70 mM KCl, 3.6 mM
411 MgCl₂, 0.1 mg/mL BSA, 1 mM BME] supplemented with 1 mM ATP, and the reaction was
412 allowed to proceed for 1 hour before being quenched with (100 ng) lambda DNA. The
413 product was run on a 6% native mini-PAGE run in 0.5X TB as has been previously reported
414 (Ranjan *et al.*, 2013).

415 The DNA binding domain (DBD) of Swc2 (residues 136-345) was cloned into a 6x
416 his-tag expression vector with a single cysteine placed directly before the N-terminus of the
417 protein for labeling purposes (**Table S2**). The Swc2 DBD was purified after expression
418 under denaturing conditions using Ni-NTA affinity purification. After purification, the
419 Swc2 DBD was specifically labeled in a 30-fold excess of Cy3-maleimide. After
420 fluorophore labeling the Swc2 DBD was Ni-NTA purified a second time to remove any
421 excess free dye. The product was then dialyzed overnight at 4C into refolding buffer
422 [20 mM Tris pH 8.0, 0.5 M NaCl, 10% Glycerol, 2 mM β-Mercaptoethanol, 0.02% NP40
423 and 1 mM PMSF] as has been previously documented (Ranjan *et al.*, 2013). Pure protein
424 was stored as aliquots at -80°C until time of use. SDS-page reveals a pure Cy3-labeled
425 product (**Figure S3**).

426 *dCas9 crRNAs, fluorescent tracrRNA annealing, and RNP assembly*

427 dCas9 was purchased from Integrated DNA Technologies (IDT), as Alt-R S.p.d
428 Cas9 Protein V3 and stored at -80°C until Ribonucleoprotein (RNP) assembly. crRNAs
429 used to target 5 sites along lambda DNA were ordered from IDT. The crRNAs used were
430 previously validated (Sternberg *et al.*, 2014) and are listed in **Table S1**. Custom 3'-amine
431 modified tracrRNA was ordered from IDT and reacted with mono-reactive NHS-ester Cy5
432 dye [Fisher Scientific cat# 45-001-190]. The labeled product was reverse-phase HPLC
433 purified. crRNA and Cy5-tracrRNA was annealed in IDT duplex buffer (cat# 11-01-03-01)
434 in equimolar amounts by heating the mixture to 95°C for 5 minutes and allowing it to cool
435 to room temperature slowly on the benchtop. RNP complexes were assembled by mixing
436 annealed guide RNA and dCas9 in a 1.5:1 molar ratio and allowing the mixture to stand at
437 room temperature for 15 minutes prior to use. Aliquoted RNPs were flash frozen and stored
438 at -80°C until time of use. Buffers for RNP assembly and cryo-storage are the same and
439 contains: 20 mM Tris-HCl pH 7.5, 200 mM KCl, 5% glycerol, and 1 mM TCEP.
440 dCas9 RNPs were diluted to 10 nM just prior to imaging in 1x NEB 3.1 (cat# B7203S).

441 *Lambda DNA preparation*

442 Biotinylated lambda DNA used in SWR1 sliding on naked DNA assays was
443 purchased from LUMICKS (SKU: 00001). Lambda DNA used in nucleosome array assays
444 was made with 3 biotins on one end, and 3 digoxigenin on the other end using the following
445 protocol. Custom oligos were ordered from IDT with sequences listed in **Table S1**. Lambda
446 DNA was ordered from NEB (cat# N3011S). Oligo 1 was annealed to lambda DNA by
447 adding a 25-fold molar excess of oligo to lambda DNA, in an annealing buffer containing
448 30 mM HEPES pH 7.5 and 100 mM KCl. This mixture was heated to 70°C for 10 minutes
449 and allowed to cool slowly to room temperature on the benchtop. 2 uL of NEB T4 DNA
450 ligase (400U, cat# M0202S) was added along with T4 DNA ligase buffer containing ATP
451 and allowed to incubate at room temperature for 30 minutes. Then 50-fold molar excess of

452 oligo 2 was added to the mixture along with an additional 1 uL of T4 DNA ligase and T4
453 DNA ligase buffer (NEB) with ATP adjusting for the change in volume and allowed to
454 incubate at room temperature for 30 minutes. The resulting mixture was heat inactivated at
455 65°C for 10 minutes. End-labeled lambda DNA was purified using Qiaex II gel-extraction
456 DNA clean-up kit following the manufactures' instructions (Qiagen cat# 20021).

457 *Lambda nucleosome array construction and validation*

458 A salt gradient dialysis approach was used to reconstitute nucleosomes onto lambda
459 DNA using methods optimized in the lab based on previously established protocols (Luger
460 et al., 1999; Vary et al., 2003). Buffers used in this reconstitution are as follows: high salt
461 buffer [10 mM Tris-HCl pH 7.5, 1 mM EDTA pH 8, 2 M NaCl, 0.02% NP-40, 5 mM
462 2-Mercaptoethanol (BME)], and low salt buffer [10 mM Tris-HCl pH 7.5, 1 mM EDTA pH
463 8, 50 mM NaCl, 0.02% NP-40, 5 mM BME]. Cy5-labeled H3 containing octamer, with the
464 same composition and preparation as previously used (Ranjan *et al.*, 2013), was titrated onto
465 the lambda DNA in the follow molar ratio to DNA: [10:1, 50:1, 100:1, 200:1, 500:1, 700:1].
466 Reconstitution reactions were prepared in 10 mM Tris pH 7.5, 1 mM EDTA pH 8,
467 0.1 mg/mL BSA Roche (cat # 10711454001), 5 mM BME. Any dilutions of octamer were
468 prepared in octamer refolding buffer: [10 mM Tris-HCl pH 7.5, 1 mM EDTA pH 8, 2 M
469 NaCl, 5 mM 2-Mercaptoethanol (BME)]. A 16-hour dialysis was set-up by placing the
470 reconstitution mixture in a 7 kDa MWCO Slide-A-Lyzer MINI Dialysis Device (Thermo
471 Scientific cat # 69560) and placed in a flotation device in high-salt buffer. Low-salt buffer
472 was slowly dripped into high-salt buffer for the duration of the dialysis with constant
473 stirring. At the end of this dialysis period, the dialysis solution was dumped and replaced
474 by 100% low-salt buffer and allowed to dialyze for an additional hour. The reconstitution
475 efficiency was first assessed using an electrophoretic mobility shift assay (EMSA)
476 (**Figure S6**). Lambda nucleosome arrays were loaded on a 0.5% agarose gel made with
477 Invitrogen UltraPure Agarose (fisher scientific cat # 16-500-500) and 0.25x TBE. Sucrose
478 loading buffer without added dyes was used to load samples on the gel. The gel was run for
479 1 hour and 45 minutes at 100V in 0.25x TBE.

480 Arrays contained a variable number of nucleosomes, where the mean number of
481 nucleosomes per array is 36 ± 15 (standard deviation) for a total of 17 arrays. The number
482 of nucleosomes per array was estimated from the length of the lambda nucleosome array at
483 5 pN force before and after nucleosome unwrapping. On average, approximately 38.6 nm
484 of lengthening at 5pN corresponded to the unwrapping of a single nucleosome, therefore
485 the difference in length before and after unwrapping was used to estimate the number of
486 nucleosomes per array.

487 *Dual optical tweezers and confocal microscope set-up and experimental workflow*

488 The LUMICKS cTrap (series G2) was used for optical tweezer experiments,
489 configured with two optical traps. The confocal imaging laser lines used were 532 nm
490 (green) and 640 nm (red) in combination with emission bandpass filters 545-620 nm (green)
491 and 650-750 nm (red). A C1 type LUMICKS microfluidics chip was used. The
492 microfluidics system was passivated at the start of each day of imaging as follows: 0.1%
493 BSA was flowed at 0.4 bar pressure for 30 minutes, followed by a 10-minute rinse with PBS
494 at 0.4 bar pressure, followed by 0.5% Pluronic F-127 flowed at 0.4 bar pressure for
495 30-minutes, followed by 30-minute rinse with PBS at 0.4 bar pressure. For SWR1 sliding
496 on naked DNA, 4.2 μm polystyrene beads coated in streptavidin (Spherotech
497 cat# SVP-40-5) were caught in each trap, and LUMICKS biotinylated lambda DNA was
498 tethered. Both traps had trap stiffness of about 0.8 pN/nm. For SWR1 sliding on lambda
499 nucleosome array, a 4.2 μm polystyrene bead coated in streptavidin was caught in trap 1,
500 and a 2.12 μm polystyrene bead coated in anti-digoxigenin antibody (Spherotech

501 cat# DIGP-20-2) was caught in trap 2 which is upstream in the path of buffer flow to trap 1.
502 For this configuration, trap 1 had a trap stiffness of about 0.3 pN/nm whereas trap 2 had a
503 trap stiffness of about 1.2 pN/nm. The presence of a single tether was confirmed by fitting
504 a force extension plot to a worm like chain model in real time while collecting data using
505 LUMICKS BlueLake software. For confocal scanning, 1.8 μ W of green and red laser power
506 were used. For most traces, the frame rate for SWR1 imaging was 50 msec, whereas for
507 Swc2 it was 20 msec. Experiments were performed at room temperature. SWR1 and Swc2
508 were both imaged in histone exchange reaction buffer [25 mM HEPES pH 7.6, 0.37 mM
509 EDTA, 5% glycerol, 0.017% NP40, 70 mM KCl, 3.6 mM MgCl₂, 0.1 mg/mL BSA, 1 mM
510 BME] made in imaging buffer. dCas9 was added to the flow chamber in Cas9 binding buffer
511 [20 mM Tris-HCl pH 8, 100 mM KCl, 5 mM MgCl₂, 5% glycerol] made in imaging buffer.
512 Imaging buffer [saturated Trolox (Millipore Sigma cat# 238813), 0.4% dextrose] is used in
513 place of water when preparing buffers. All buffers were filter sterilized with a 0.2 μ m filter
514 prior to use.

515 *TIRF based binding kinetics assay and analysis*

516 We co-localized SWR1 binding to Cy5-labeled dsDNAs of different lengths for real-
517 time binding kinetic measurements (**Figure S1D-E**). These experiments were all conducted
518 using flow cells made with PEG-passivated quartz slides using previously detailed methods
519 (Roy et al., 2008). The appropriate biotinylated Cy5-labeled DNA was immobilized on the
520 surface of the PEG-passivated quartz slide using neutravidin. After DNA immobilization,
521 the channels of the flow cell were washed to remove free DNA and imaging buffer was
522 flowed into the channel. Next, 5 nM Cy5-SWR1 in imaging buffer was flowed into the
523 channel immediately after starting image acquisition. A standard smFRET imaging buffer
524 with oxygen scavenging system was used as has been previously established (Joo and Ha,
525 2012). The first 10 frames (1s) of each imaging experiment were collected using
526 Cy5-excitation so that all Cy5-DNA spots could be identified. The remaining 299 seconds
527 of the movie were collected under Cy3-excitation so that Cy3-SWR1 could be imaged. Data
528 analysis was carried out using homemade IDL scripts for image analysis and MATLAB
529 scripts for data analysis. The data was analyzed so that all the Cy5-DNA molecules in an
530 image were identified from the first second of the movie under Cy5-excitation. Next, the
531 Cy3 intensity was monitored for the remainder of the movie for each DNA molecule. SWR1
532 binding to nucleosomes was detected by a sharp increase in Cy3 signal in spots that had
533 Cy5 signal.

534 The on-rate was defined as the time between when Cy3-SWR1 was injected into the
535 imaging chamber to when Cy3-SWR1 first bound to a specific DNA molecule resulting in
536 an increase in Cy3 intensity. The off-rate was defined as the length of time Cy3-SWR1
537 was bound to a DNA molecule which is the duration of the high Cy3 fluorescence state. While
538 only one on-rate measurement could be conducted for one DNA molecule, multiple off-rate
539 measurements could be made as one DNA molecule was subjected to multiple Cy3-SWR1
540 binding events. Binding events where more than one SWR1 were bound to the DNA were
541 excluded from the off-rate analysis. Off-rate measurements under different laser intensities
542 were made by measuring the laser power immediately prior to the imaging experiment
543 (**Figure S1C**). All experiments were conducted using imaging channels from the same
544 quartz slide to minimize differences in laser intensity that can result from changes in shape
545 of the TIRF spot.

546 *Single particle tracking and data analysis*

547 LUMICKS BlueLake HDF5 data files were initially processed using the commercial
548 Pylake Python package to extract kymograph pixel intensities along with corresponding
549 metadata. Particle tracking was then performed in MATLAB (MathWorks). First, spatially
550 well-separated particles were individually segmented from full-length kymographs

551 containing multiple diffusing particles. Next, for each time-step, a one-dimensional
552 gaussian was fit to the pixel intensities to extract the centroid position of the particle in time.
553 Then the MSD for each time-lag was calculated using:

$$554 \quad MSD(n, N) = \sum_{i=1}^{N-n} \frac{(X_{i+n} - X_i)^2}{N - n}$$

555 where N is the total number of frames in the trace, n is the size of the time lag over which
556 the MSD is calculated, i is the sliding window over which displacement is measured, X is the
557 position of the particle. Since particles exhibit Brownian diffusion, the diffusion coefficient
558 for each particle was then calculated from a linear fit to the initial portion of the mean
559 squared displacement (MSD) versus time lag plot by solving for D using: $MSD = 2Dt$.

560 For the linear fit, the number of points included varied to optimize for a maximal
561 number of points fit with the highest Pearson correlation (r^2) and a p-value lower than 0.01.
562 For particles where this initial best fit could not be found, the first 25% of the trace was
563 linearly fit. Fits that produced negative slope values corresponded to traces where particles
564 are immobile; to reflect this, negative slopes were given a slope of 0. Finally, outlier traces
565 with diffusion coefficients greater than $0.14 \mu\text{m}^2/\text{s}$ for SWR1 or $5 \mu\text{m}^2/\text{s}$ for Swc2 were
566 dropped; in every case this consisted of less than 3% of all traces. The distribution of
567 diffusion coefficients estimated using this method was almost identical to what is produced
568 using an alternative method which extracts diffusion coefficients using a linear fit from time
569 lags 3-10 rejecting fits with $r^2 < 0.9$ (Tafvizi *et al.*, 2008) (**Figure S8**). A summary of
570 statistics as well as criteria for excluding traces is provided in **Table S3**. We estimated the
571 localization precision using the following formula:

$$572 \quad \sigma^2 = \left[\frac{s^2}{N} + \frac{a^2/12}{N} + \frac{8\pi s^4 b^4}{a^2 N^2} \right] \quad \text{Equation 2}$$

573 where N is the number of photons collected which was on average 12.9 photons per 5-pixel
574 window surrounding the centroid (see **Figure S9**); s is the standard deviation of the
575 microscope point-spread function, 294 nm; a is the pixel size, 100 nm; and b is the
576 background intensity which was on average 0.8 photons per 5-pixel window. This results in
577 a $\sigma = 82$ nm.

578 *Calculation of theoretical maximal hydrodynamic diffusion coefficients*

579 The radius of gyration of SWR1 and Swc2 were calculated using the following formulas.
580 First, the volume (V) of each particle was estimated using the following equation:

$$581 \quad V(\text{nm}^3) = \frac{\left(\left(0.73 \frac{\text{cm}^3}{\text{g}} \right) \left(10^{21} \frac{\text{nm}^3}{\text{cm}^3} \right) \right)}{6.023 * 10^{23} \frac{\text{Da}}{\text{g}}} * M(\text{Da}) \quad \text{Equation 3}$$

582 Then, the radius of gyration was estimated using the following equation:

$$583 \quad R_{min} = \left(\frac{3V}{4\pi} \right)^{\frac{1}{3}} \quad \text{Equation 4}$$

584 where M is mass in Daltons (Erickson, 2009). Given the input of 1 MDa for SWR1 and
585 25.4 kDa for Swc2, the resulting radii of gyration are 6.62 nm SWR1 and 1.94 nm for Swc2.
586 Next, the theoretical upper limit of 1D diffusion with no rotation was calculated using the
587 following formula:

$$588 \quad D = \frac{k_b T}{f} \quad \text{Equation 5}$$

589 Where:

$$590 \quad f = 6\pi\eta R \quad \text{Equation 6}$$

591 and η is the viscosity 9×10^{-10} pN*s/nm² (Schurr, 1979). The resulting upper limit without
592 rotation for SWR1, is $36.7 \mu\text{m}^2/\text{s}$ and for Swc2 it is $125 \mu\text{m}^2/\text{s}$. When computing the upper
593 limit of 1D diffusion with rotation, the following formula considers the energy dissipation
594 that comes from rotating while diffusing:

$$595 \quad f = 6\pi\eta R + \left(\frac{2\pi}{10BP}\right)^2 [8\pi\eta R^3 + 6\pi\eta R(R_{oc})^2] \quad \text{Equation 7}$$

596 where R_{oc} is the distance between the center of mass of the DNA and the bound protein, and
597 10 BP is the length of one helical turn or 3.4 nm (Ahmadi *et al.*, 2018; Bagchi *et al.*, 2008;
598 Blainey *et al.*, 2009). Since we do not have structures of SWR1 or Swc2 bound to dsDNA
599 alone, we report both the maximal and minimal value of the theoretical upper limit, where
600 the minimal value corresponds to $R_{oc} = R$ and the maximal value corresponds to $R_{oc} = 0$.
601 For SWR1 this minimum value is $0.105 \mu\text{m}^2/\text{s}$ and the maximum value is $0.183 \mu\text{m}^2/\text{s}$
602 whereas for Swc2 this minimum value is $4.01 \mu\text{m}^2/\text{s}$ and the maximum value is $6.86 \mu\text{m}^2/\text{s}$.

603 Scanning speed estimation

604 Lambda DNA tethered at its ends to two optically trapped beads was pulled to a tension of
605 5 pN, which resulted in a length approximately 92% of its contour length (15.2 μm). The
606 length per base pair of DNA, 0.31 nm, is therefore slightly shorter than the value at full
607 contour length (Baumann *et al.*, 2000). The length of the NDR, 150 bp, in our conditions
608 is therefore roughly 0.047 μm long. Since our localization precision is low, ~ 82 nm (see
609 **Equation 2**), we do not have diffusion information at the resolution of base pairs, and
610 therefore do not consider discrete models to approximate scanning speed. Given a median
611 diffusion coefficient of SWR1 in the presence of 1 mM ATP of $0.024 \mu\text{m}^2/\text{sec}$, and the one-
612 dimensional translational diffusion, $l = 2Dt$, where l is the length in μm of DNA, we can
613 approximate the time required to scan this length of DNA to be 0.093 seconds assuming a
614 continuous model (Berg, 1983).

615 References

617 Reference List

- 619 Ahmadi, A., Rosnes, I., Blicher, P., Diekmann, R., Schüttpelz, M., Glette, K., Tørresen, J., Bjørås,
620 M., Dalhus, B., and Rowe, A.D. (2018). Breaking the speed limit with multimode fast scanning of
621 DNA by Endonuclease V. *Nature Communications* 9. [10.1038/s41467-018-07797-4](https://doi.org/10.1038/s41467-018-07797-4).
622 Albert, I., Mavrich, T.N., Tomsho, L.P., Qi, J., Zanton, S.J., Schuster, S.C., and Pugh, B.F.
623 (2007). Translational and rotational settings of H2A.Z nucleosomes across the *Saccharomyces*
624 *cerevisiae* genome. *Nature* 446, 572-576. [10.1038/nature05632](https://doi.org/10.1038/nature05632).
625 Bagchi, B., Blainey, P.C., and Xie, X.S. (2008). Diffusion constant of a nonspecifically bound
626 protein undergoing curvilinear motion along DNA. *J Phys Chem B* 112, 6282-6284.
627 [10.1021/jp077568f](https://doi.org/10.1021/jp077568f).

- 628 Baumann, C.G., Bloomfield, V.A., Smith, S.B., Bustamante, C., Wang, M.D., and Block, S.M.
629 (2000). Stretching of single collapsed DNA molecules. *Biophys J* 78, 1965-1978. 10.1016/S0006-
630 3495(00)76744-0.
- 631 Berg, H.C. (1983). *Random Walks in Biology* (Princeton University Press).
- 632 Berg, O.G., Winter, R.B., and Von Hippel, P.H. (1981). Diffusion-driven mechanisms of protein
633 translocation on nucleic acids. 1. Models and theory. *Biochemistry* 20, 6929-6948.
634 10.1021/bi00527a028.
- 635 Bernstein, B.E., Liu, C., Humphrey, E.L., Perlstein, E.O., and Schreiber, S.L. (2004). Global
636 nucleosome occupancy in yeast. *Genome Biology* 5, R62. 10.1186/gb-2004-5-9-r62.
- 637 Beyer, D.C., Ghoneim, M.K., and Spies, M. (2013). Structure and Mechanisms of SF2 DNA
638 Helicases. In (Springer New York), pp. 47-73. 10.1007/978-1-4614-5037-5_3.
- 639 Blainey, P.C., Luo, G., Kou, S.C., Mangel, W.F., Verdine, G.L., Bagchi, B., and Xie, X.S. (2009).
640 Nonspecifically bound proteins spin while diffusing along DNA. *Nat Struct Mol Biol* 16, 1224-
641 1229. 10.1038/nsmb.1716.
- 642 Blainey, P.C., van Oijen, A.M., Banerjee, A., Verdine, G.L., and Xie, X.S. (2006). A base-
643 excision DNA-repair protein finds intrahelical lesion bases by fast sliding in contact with DNA.
644 *Proc Natl Acad Sci U S A* 103, 5752-5757. 10.1073/pnas.0509723103.
- 645 Bonnet, I., Biebricher, A., Porte, P.L., Loverdo, C., Benichou, O., Voituriez, R., Escude, C.,
646 Wende, W., Pingoud, A., and Desbiolles, P. (2008). Sliding and jumping of single EcoRV
647 restriction enzymes on non-cognate DNA. *Nucleic Acids Res* 36, 4118-4127.
648 10.1093/nar/gkn376.
- 649 Brouwer, I., Sitters, G., Candelli, A., Heerema, S.J., Heller, I., de Melo, A.J., Zhang, H.,
650 Normanno, D., Modesti, M., Peterman, E.J., and Wuite, G.J. (2016). Sliding sleeves of XRCC4-
651 XLF bridge DNA and connect fragments of broken DNA. *Nature* 535, 566-569.
652 10.1038/nature18643.
- 653 Brower-Toland, B.D., Smith, C.L., Yeh, R.C., Lis, J.T., Peterson, C.L., and Wang, M.D. (2002).
654 Mechanical disruption of individual nucleosomes reveals a reversible multistage release of DNA.
655 *Proceedings of the National Academy of Sciences* 99, 1960-1965. 10.1073/pnas.022638399.
- 656 Brown, M.W., Kim, Y., Williams, G.M., Huck, J.D., Surtees, J.A., and Finkelstein, I.J. (2016).
657 Dynamic DNA binding licenses a repair factor to bypass roadblocks in search of DNA lesions.
658 *Nat Commun* 7, 10607. 10.1038/ncomms10607.
- 659 Chereji, R.V., Ramachandran, S., Bryson, T.D., and Henikoff, S. (2018). Precise genome-wide
660 mapping of single nucleosomes and linkers in vivo. *Genome Biology* 19. 10.1186/s13059-018-
661 1398-0.
- 662 Elf, J., Li, G.W., and Xie, X.S. (2007). Probing transcription factor dynamics at the single-
663 molecule level in a living cell. *Science* 316, 1191-1194. 10.1126/science.1141967.
- 664 Erickson, H.P. (2009). Size and Shape of Protein Molecules at the Nanometer Level Determined
665 by Sedimentation, Gel Filtration, and Electron Microscopy. *Biological Procedures Online* 11, 32-
666 51. 10.1007/s12575-009-9008-x.
- 667 Fierz, B., and Poirier, M.G. (2019). Biophysics of Chromatin Dynamics. *Annu Rev Biophys* 48,
668 321-345. 10.1146/annurev-biophys-070317-032847.
- 669 Giaimo, B.D., Ferrante, F., Herchenröther, A., Hake, S.B., and Borggrefe, T. (2019). The histone
670 variant H2A.Z in gene regulation. *Epigenetics & Chromatin* 12. 10.1186/s13072-019-0274-9.
- 671 Gorman, J., Chowdhury, A., Surtees, J.A., Shimada, J., Reichman, D.R., Alani, E., and Greene,
672 E.C. (2007). Dynamic basis for one-dimensional DNA scanning by the mismatch repair complex
673 Msh2-Msh6. *Mol Cell* 28, 359-370. 10.1016/j.molcel.2007.09.008.
- 674 Gorman, J., Plys, A.J., Visnapuu, M.L., Alani, E., and Greene, E.C. (2010). Visualizing one-
675 dimensional diffusion of eukaryotic DNA repair factors along a chromatin lattice. *Nat Struct Mol*
676 *Biol* 17, 932-938. 10.1038/nsmb.1858.

- 677 Gruszka, D.T., Xie, S., Kimura, H., and Yardimci, H. (2020). Single-molecule imaging reveals
678 control of parental histone recycling by free histones during DNA replication. *Sci Adv* 6.
679 10.1126/sciadv.abc0330.
- 680 Gutierrez-Escribano, P., Newton, M.D., Llauro, A., Huber, J., Tanasie, L., Davy, J., Aly, I.,
681 Aramayo, R., Montoya, A., Kramer, H., et al. (2019). A conserved ATP- and Scc2/4-dependent
682 activity for cohesin in tethering DNA molecules. *Sci Adv* 5, eaay6804. 10.1126/sciadv.aay6804.
- 683 Hannon, R., Richards, E.G., and Gould, H.J. (1986). Facilitated diffusion of a DNA binding
684 protein on chromatin. *The EMBO Journal* 5, 3313-3319. 10.1002/j.1460-2075.1986.tb04645.x.
- 685 Hedglin, M., and O'Brien, P.J. (2010). Hopping Enables a DNA Repair Glycosylase To Search
686 Both Strands and Bypass a Bound Protein. *ACS Chemical Biology* 5, 427-436.
687 10.1021/cb1000185.
- 688 Heller, I., Hoekstra, T.P., King, G.A., Peterman, E.J., and Wuite, G.J. (2014a). Optical tweezers
689 analysis of DNA-protein complexes. *Chem Rev* 114, 3087-3119. 10.1021/cr4003006.
- 690 Heller, I., Sitters, G., Broekmans, O.D., Biebricher, A.S., Wuite, G.J., and Peterman, E.J. (2014b).
691 Mobility analysis of super-resolved proteins on optically stretched DNA: comparing imaging
692 techniques and parameters. *Chemphyschem* 15, 727-733. 10.1002/cphc.201300813.
- 693 Jiang, C., and Pugh, B.F. (2009). A compiled and systematic reference map of nucleosome
694 positions across the *Saccharomyces cerevisiae* genome. *Genome Biol* 10, R109. 10.1186/gb-
695 2009-10-10-r109.
- 696 Joo, C., and Ha, T. (2012). Single-molecule FRET with total internal reflection microscopy. *Cold*
697 *Spring Harb Protoc* 2012. 10.1101/pdb.top072058.
- 698 Kamagata, K., Ouchi, K., Tan, C., Mano, E., Mandal, S., Wu, Y., Takada, S., Takahashi, S., and
699 Johnson, R.C. (2020). The HMGB chromatin protein Nhp6A can bypass obstacles when traveling
700 on DNA. *Nucleic Acids Research* 48, 10820-10831. 10.1093/nar/gkaa799.
- 701 Kim, J.M., Visanpattanasin, P., Jou, V., Liu, S., Tang, X., Zheng, Q., Li, K.Y., Snedeker, J.,
702 Lavis, L.D., Lionnet, T., and Wu, C. (2021). Single-molecule imaging of chromatin remodelers
703 reveals role of ATPase in promoting fast kinetics of target search and dissociation from
704 chromatin. *eLife* 10. 10.7554/elife.69387.
- 705 Kubik, S., Bruzzone, M.J., Challal, D., Dreos, R., Mattarocci, S., Bucher, P., Libri, D., and Shore,
706 D. (2019). Opposing chromatin remodelers control transcription initiation frequency and start site
707 selection. *Nat Struct Mol Biol* 26, 744-754. 10.1038/s41594-019-0273-3.
- 708 Kubik, S., Bruzzone, M.J., Jacquet, P., Falcone, J.L., Rougemont, J., and Shore, D. (2015).
709 Nucleosome Stability Distinguishes Two Different Promoter Types at All Protein-Coding Genes
710 in Yeast. *Mol Cell* 60, 422-434. 10.1016/j.molcel.2015.10.002.
- 711 Lee, W., Tillo, D., Bray, N., Morse, R.H., Davis, R.W., Hughes, T.R., and Nislow, C. (2007). A
712 high-resolution atlas of nucleosome occupancy in yeast. *Nature Genetics* 39, 1235-1244.
713 10.1038/ng2117.
- 714 Luger, K., Rechsteiner, T.J., and Richmond, T.J. (1999). Expression and Purification of
715 Recombinant Histones and Nucleosome Reconstitution. In (Humana Press), pp. 1-16. 10.1385/1-
716 59259-681-9:1.
- 717 Luk, E., Ranjan, A., Fitzgerald, P.C., Mizuguchi, G., Huang, Y., Wei, D., and Wu, C. (2010).
718 Stepwise histone replacement by SWR1 requires dual activation with histone H2A.Z and
719 canonical nucleosome. *Cell* 143, 725-736. 10.1016/j.cell.2010.10.019.
- 720 Marklund, E., van Oosten, B., Mao, G., Amselem, E., Kipper, K., Sabantsev, A., Emmerich, A.,
721 Globisch, D., Zheng, X., Lehmann, L.C., et al. (2020). DNA surface exploration and operator
722 bypassing during target search. *Nature*. 10.1038/s41586-020-2413-7.
- 723 Mirny, L., Slutsky, M., Wunderlich, Z., Tafvizi, A., Leith, J., and Kosmrlj, A. (2009). How a
724 protein searches for its site on DNA: the mechanism of facilitated diffusion. *JOURNAL OF*
725 *PHYSICS A: MATHEMATICAL AND THEORETICAL* 42. 10.1088/1751-8113/42.

- 726 Newton, M.D., Taylor, B.J., Driessen, R.P.C., Roos, L., Cveticic, N., Allyjaun, S., Lenhard, B.,
727 Cuomo, M.E., and Rueda, D.S. (2019). DNA stretching induces Cas9 off-target activity. *Nat*
728 *Struct Mol Biol* *26*, 185-192. 10.1038/s41594-019-0188-z.
- 729 Nguyen, V.Q., Ranjan, A., Liu, S., Tang, X., Ling, Y.H., Wisniewski, J., Mizuguchi, G., Li, K.Y.,
730 Jou, V., Zheng, Q., et al. (2021). Spatiotemporal coordination of transcription preinitiation
731 complex assembly in live cells. *Molecular Cell* *81*, 3560-3575.e3566.
732 10.1016/j.molcel.2021.07.022.
- 733 Nodelman, I.M., and Bowman, G.D. (2021). Biophysics of Chromatin Remodeling. *Annu Rev*
734 *Biophys* *50*, 73-93. 10.1146/annurev-biophys-082520-080201.
- 735 Nodelman, I.M., Patel, A., Levendosky, R.F., and Bowman, G.D. (2020). Reconstitution and
736 Purification of Nucleosomes with Recombinant Histones and Purified DNA. *Curr Protoc Mol*
737 *Biol* *133*, e130. 10.1002/cpmb.130.
- 738 Park, S., Lee, O.C., Durang, X., and Jeon, J.-H. (2021). A mini-review of the diffusion dynamics
739 of DNA-binding proteins: experiments and models. *Journal of the Korean Physical Society* *78*,
740 408-426. 10.1007/s40042-021-00060-y.
- 741 Porecha, R.H., and Stivers, J.T. (2008). Uracil DNA glycosylase uses DNA hopping and short-
742 range sliding to trap extrahelical uracils. *Proceedings of the National Academy of Sciences* *105*,
743 10791-10796. 10.1073/pnas.0801612105.
- 744 Poyton, M.F., Feng, X.A., Ranjan, A., Lei, Q., Wang, F., Zarb, J.S., Louder, R.K., Park, G., Jo,
745 M.H., Ye, J., et al. (2021). Coordinated DNA and Histone Dynamics Drive Accurate Histone
746 H2A.Z Exchange. *bioRxiv*, 2021.2010.2022.465479. 10.1101/2021.10.22.465479.
- 747 Raisner, R.M., Hartley, P.D., Meneghini, M.D., Bao, M.Z., Liu, C.L., Schreiber, S.L., Rando,
748 O.J., and Madhani, H.D. (2005). Histone variant H2A.Z marks the 5' ends of both active and
749 inactive genes in euchromatin. *Cell* *123*, 233-248. 10.1016/j.cell.2005.10.002.
- 750 Ranjan, A., Mizuguchi, G., FitzGerald, P.C., Wei, D., Wang, F., Huang, Y., Luk, E., Woodcock,
751 C.L., and Wu, C. (2013). Nucleosome-free region dominates histone acetylation in targeting
752 SWR1 to promoters for H2A.Z replacement. *Cell* *154*, 1232-1245. 10.1016/j.cell.2013.08.005.
- 753 Ranjan, A., Nguyen, V.Q., Liu, S., Wisniewski, J., Kim, J.M., Tang, X., Mizuguchi, G., Elalaoui,
754 E., Nickels, T.J., Jou, V., et al. (2020). Live-cell single particle imaging reveals the role of RNA
755 polymerase II in histone H2A.Z eviction. *Elife* *9*. 10.7554/eLife.55667.
- 756 Rhee, H.S., Bataille, A.R., Zhang, L., and Pugh, B.F. (2014). Subnucleosomal structures and
757 nucleosome asymmetry across a genome. *Cell* *159*, 1377-1388. 10.1016/j.cell.2014.10.054.
- 758 Rhee, H.S., and Pugh, B.F. (2012). Genome-wide structure and organization of eukaryotic pre-
759 initiation complexes. *Nature* *483*, 295-301. 10.1038/nature10799.
- 760 Ricchetti, M., Metzger, W., and Heumann, H. (1988). One-dimensional diffusion of *Escherichia*
761 *coli* DNA-dependent RNA polymerase: a mechanism to facilitate promoter location. *Proceedings*
762 *of the National Academy of Sciences* *85*, 4610-4614. 10.1073/pnas.85.13.4610.
- 763 Rill, N., Mukhortava, A., Lorenz, S., and Tessmer, I. (2020). Alkyltransferase-like protein
764 clusters scan DNA rapidly over long distances and recruit NER to alkyl-DNA lesions.
765 *Proceedings of the National Academy of Sciences* *117*, 9318-9328. 10.1073/pnas.1916860117.
- 766 Roy, R., Hohng, S., and Ha, T. (2008). A practical guide to single-molecule FRET. *Nat Methods*
767 *5*, 507-516. 10.1038/nmeth.1208.
- 768 Rudnizky, S., Bavly, A., Malik, O., Pnueli, L., Melamed, P., and Kaplan, A. (2016). H2A.Z
769 controls the stability and mobility of nucleosomes to regulate expression of the LH genes. *Nat*
770 *Commun* *7*, 12958. 10.1038/ncomms12958.
- 771 Schurr, J.M. (1979). The one-dimensional diffusion coefficient of proteins absorbed on DNA.
772 *Biophysical Chemistry* *9*, 413-414. 10.1016/0301-4622(75)80057-3.
- 773 Singh, D., Sternberg, S.H., Fei, J., Doudna, J.A., and Ha, T. (2016). Real-time observation of
774 DNA recognition and rejection by the RNA-guided endonuclease Cas9. *Nat Commun* *7*, 12778.
775 10.1038/ncomms12778.

- 776 Slutsky, M., and Mirny, L.A. (2004). Kinetics of protein-DNA interaction: Facilitated target
777 location in sequence-dependent potential. *Biophysical Journal* *87*, 4021-4035.
778 10.1529/biophysj.104.050765.
- 779 Sternberg, S.H., Redding, S., Jinek, M., Greene, E.C., and Doudna, J.A. (2014). DNA
780 interrogation by the CRISPR RNA-guided endonuclease Cas9. *Nature* *507*, 62-67.
781 10.1038/nature13011.
- 782 Sun, L., Pierrakeas, L., Li, T., and Luk, E. (2020). Thermosensitive Nucleosome Editing Reveals
783 the Role of DNA Sequence in Targeted Histone Variant Deposition. *Cell Rep* *30*, 257-268 e255.
784 10.1016/j.celrep.2019.12.006.
- 785 Tafvizi, A., Huang, F., Fersht, A.R., Mirny, L.A., and van Oijen, A.M. (2011). A single-molecule
786 characterization of p53 search on DNA. *Proc Natl Acad Sci U S A* *108*, 563-568.
787 10.1073/pnas.1016020107.
- 788 Tafvizi, A., Huang, F., Leith, J.S., Fersht, A.R., Mirny, L.A., and van Oijen, A.M. (2008). Tumor
789 suppressor p53 slides on DNA with low friction and high stability. *Biophys J* *95*, L01-03.
790 10.1529/biophysj.108.134122.
- 791 Tessarz, P., and Kouzarides, T. (2014). Histone core modifications regulating nucleosome
792 structure and dynamics. *Nature Reviews Molecular Cell Biology* *15*, 703-708. 10.1038/nrm3890.
- 793 Tramantano, M., Sun, L., Au, C., Labuz, D., Liu, Z., Chou, M., Shen, C., and Luk, E. (2016).
794 Constitutive turnover of histone H2A.Z at yeast promoters requires the preinitiation complex.
795 *Elife* *5*. 10.7554/eLife.14243.
- 796 Vary, J.C., Fazio, T.G., and Tsukiyama, T. (2003). Assembly of Yeast Chromatin Using ISWI
797 Complexes. In (Elsevier), pp. 88-102. 10.1016/s0076-6879(03)75006-x.
- 798 Vestergaard, C.L., Blainey, P.C., and Flyvbjerg, H. (2018). Single-particle trajectories reveal two-
799 state diffusion-kinetics of hOGG1 proteins on DNA. *Nucleic Acids Res* *46*, 2446-2458.
800 10.1093/nar/gky004.
- 801 Visnapuu, M.-L., and Greene, E.C. (2009). Single-molecule imaging of DNA curtains reveals
802 intrinsic energy landscapes for nucleosome deposition. *Nature Structural & Molecular Biology*
803 *16*, 1056-1062. 10.1038/nsmb.1655.
- 804 Von Hippel, P.H., and Berg, O.G. (1989). Facilitated Target Location in Biological Systems.
805 *Journal of Biological Chemistry* *264*, 675-678. 10.1016/s0021-9258(19)84994-3.
- 806 Wasserman, M.R., Schauer, G.D., O'Donnell, M.E., and Liu, S. (2019). Replication Fork
807 Activation Is Enabled by a Single-Stranded DNA Gate in CMG Helicase. *Cell* *178*, 600-611 e616.
808 10.1016/j.cell.2019.06.032.
- 809 Watanabe, S., Radman-Livaja, M., Rando, O.J., and Peterson, C.L. (2013). A histone acetylation
810 switch regulates H2A.Z deposition by the SWR-C remodeling enzyme. *Science* *340*, 195-199.
811 10.1126/science.1229758.
- 812 Willhoft, O., Ghoneim, M., Lin, C.L., Chua, E.Y.D., Wilkinson, M., Chaban, Y., Ayala, R.,
813 McCormack, E.A., Ocloo, L., Rueda, D.S., and Wigley, D.B. (2018). Structure and dynamics of
814 the yeast SWR1-nucleosome complex. *Science* *362*. 10.1126/science.aat7716.
- 815 Xu, Z., Wei, W., Gagneur, J., Perocchi, F., Clauder-Münster, S., Camblong, J., Guffanti, E., Stutz,
816 F., Huber, W., and Steinmetz, L.M. (2009). Bidirectional promoters generate pervasive
817 transcription in yeast. *Nature* *457*, 1033-1037. 10.1038/nature07728.
- 818 Yan, L., and Chen, Z. (2020). A Unifying Mechanism of DNA Translocation Underlying
819 Chromatin Remodeling. *Trends Biochem Sci* *45*, 217-227. 10.1016/j.tibs.2019.09.002.
- 820 Yen, K., Vinayachandran, V., Batta, K., Koerber, R.T., and Pugh, B.F. (2012). Genome-wide
821 nucleosome specificity and directionality of chromatin remodelers. *Cell* *149*, 1461-1473.
822 10.1016/j.cell.2012.04.036.
- 823 Yen, K., Vinayachandran, V., and Pugh, B.F. (2013). SWR-C and INO80 chromatin remodelers
824 recognize nucleosome-free regions near +1 nucleosomes. *Cell* *154*, 1246-1256.
825 10.1016/j.cell.2013.08.043.

826 Yuan, G.C. (2005). Genome-Scale Identification of Nucleosome Positions in *S. cerevisiae*.
827 *Science* 309, 626-630. 10.1126/science.1112178.
828 Zhang, H., Roberts, D.N., and Cairns, B.R. (2005). Genome-wide dynamics of Htz1, a histone
829 H2A variant that poises repressed/basal promoters for activation through histone loss. *Cell* 123,
830 219-231. 10.1016/j.cell.2005.08.036.

831
832

833 **Acknowledgments**

834
835

Competing interests:

836 The authors declare that they have no conflict of interest.

837
838

Funding:

839 This work was supported by the NIH Grant S10 025221 (Institute: Office of the Director
840 [OD], Office of Research Infrastructure Programs [ORIP]) (cTrap grant core-facilities JHU
841 SOM), a National Science Foundation, Graduate Research Fellowship Program DGE-
842 1746891(to C.C.C.), a National Institutes of Health training grant T32 GM007445(to
843 C.C.C.) and a National Institutes of Health Postdoctoral Training Fellowship F32
844 GM128299 (to M.F.P.).

845
846

Author contributions:

847 C.C.C., M.F.P. C.W. and T.H. conceived the project. C.C.C. designed, performed, and
848 analyzed cTrap experiments, M.F.P. designed, performed, and analyzed TIRF experiments.
849 G.P. and R.K.L. purified site specifically labeled SWR1, M.F.P. purified Swc2. T.Z.
850 assisted with cTrap measurements. C.C.C. wrote the manuscript with contributions from all
851 authors. C.W. and T.H. supervised the project.

852
853

Acknowledgements:

854 We thank Dr. Kelsey Bettridge for providing a template script for single particle tracking in
855 Matlab.

856
857

Data and materials availability:

858 Data is available from authors upon request. Matlab and Python scripts used in processing
859 the data are also available upon request.